Robust Neural Decoding with low-density EEG

Ling Huang[1,2,3*], Manuel Varlet[4,5], Tijl Grootswagers[4,6]

[1]Key Laboratory of Brain, Cognition and Education Sciences, Ministry of Education, South China Normal University, Guangzhou, , China. [2]School of Psychology, Center for Studies of Psychological Application, and Guangdong Provincial Key Laboratory of Mental Health and Cognitive Science, South China Normal University, Guangzhou, China. [3]Department of Psychology, The Ohio State University, Columbus, USA. [4]The MARCS institute for Brain, Behaviour and Development, Western Sydney University, Sydney, Australia. [5]School of Psychology, Western Sydney University, Sydney, Australia. [6]School of Computer, Data, and Mathematical Sciences, Western Sydney University, Sydney, Australia.

*Correspondence: huang.5901@osu.edu

Ling Huang, PhD

Department of Psychology, The Ohio State University, Columbus, USA

Abstract

High-density EEG recording enhances spatial resolution for neural signal decoding, yet the relationship between electrode density and decoding performance, as well as the minimum number of electrodes required for effective decoding, remains unclear. To address this, we systematically investigated the decoding accuracy of neural signals across varying electrode densities (16, 32, 64, 96, and 128 electrodes) using visual grating stimuli characterized by orientation, contrast, spatial frequency, and color. Our findings showed that accurate decoding of these visual grating features was achievable even with as few as 16 electrodes, highlighting the robustness of decodable neural signals. To test the generalization of these results to more complex natural stimuli, we conducted a similar analysis with a diverse set of naturalistic images categorizable into living/non-living and moving/non-moving. The results consistently showed that effective decoding persists even with only 16 electrodes, demonstrating robust decoding efficacy even for complex naturalistic stimuli. This work provides valuable insights into the efficient neural decoding offered by low-density EEG and robustness of neural signal representation.

Keywords: low-density EEG; neural decoding; electrode density; decoding accuracy; stimulus generalization

1. **Introduction**

Electroencephalography (EEG) is a widely used non-invasive technique with high temporal resolution that has become a valuable tool for neuroimaging studies[1]. In particular, it is extensively used in visual studies to investigate cognitive processes such as object recognition, spatial attention, working memory, and motion perception[2-7]. Numerous studies using diverse visual stimuli, from simple gratings to natural scenes, suggest that EEG signals encode rich information about both low- and high-level visual representations[4-7].

Despite these versatile neural representations across stimulus types, the extent to which the number of electrodes affects decoding performance remains controversial[8-10]. With the advancement of EEG technology, the number of electrodes used in recording has steadily increased, leading to the development of high-density EEG systems. Generally, these systems offer enhanced spatial resolution and improved neural signal decoding capabilitie[10,11]. However, this does not mean that lower-density EEG cannot support meaningful decoding. Recent studies have suggested that image classification, image reconstruction, and functional connectivity analysis may still be feasible using low-density EEG, challenging the assumption that more electrodes necessarily yield accurate visual decoding performance[8,9,12].

From a neurophysiological perspective, this possibility is supported by the biophysical properties of EEG. Although EEG signals originate from anatomically localized sources, such as early visual areas in the occipital cortex involved in encoding low-level features[13], the resulting scalp potentials are shaped by volume conduction, which causes neural activity to spread through the brain and skull. This process produces spatially widespread but locally enhanced scalp fields[14-17]. As a result, sparse but broadly distributed EEG montages, when designed to preserve full-head coverage, may still capture the key components of multivariate signal patterns, allowing even low-density electrode configurations to retain sufficient information for reliable decoding[8,9,12,18].

Moreover, deploying high-density EEG is associated with several limitations, including high costs, extensive setup time, lack of portability, and substantial

computational demands[8,9,12]. In contrast, low-density EEG has been shown to be effective in brain-computer interface (BCI) applications, particularly among individuals with motor disabilities[19]. In clinical practice, especially in epileptology, low-density EEG is routinely used, with 9 to 21 electrodes commonly employed for diagnostic purposes[20,21]. These observations raise a critical question: can comparable decoding performance be achieved with a reduced number of electrodes, thereby making EEG-based decoding more practical and widely accessible?

To address this issue, we systematically investigated the impact of electrode density on visual decoding performance. Using a publicly available EEG dataset[22] featuring visual grating stimuli varying in orientation, contrast, spatial frequency, and color, we examined decoding accuracy across different electrode densities (16, 32, 64, 96, and 128 electrodes). Our findings revealed that accurate decoding of visual grating features could be achieved even with as few as 16 electrodes, demonstrating the robustness of neural signal representation. To assess the generalizability of these results, we extended our analysis to a diverse set of natural images from another publicly available EEG dataset[23]. This dataset included visual image categories such as living animals (whales), living plants (flowers), non-living moving artificial objects (trains), non-living moving natural objects (waterfalls), non-living still artificial objects (cups), and non-living still natural objects (rocks). Using these natural stimuli, we again found that decoding performance remained robust even with as few as 16 electrodes, suggesting that high-level visual information can also be reliably captured with low-density EEG. The consistency of decoding performance across these varied stimulus types further reinforces the notion that effective neural decoding is achievable with low-density EEG.

2. Methods

This study utilized publicly available datasets from OpenNeuro: Experiment 1 (https://doi.org/10.18112/openneuro.ds004357.v1.0.1) and Experiment 2 (https://doi.org/10.18112/openneuro.ds003885.v1.0.7). In Experiment 1, participants were presented with oriented grating stimuli, shown for one frame (16.67 ms) in sequences at 6.67 Hz (133 ms ISI; 150 ms SOA) or 20 Hz (33 ms ISI; 50 ms SOA), and were asked to fixate on a black bullseye and detect when the fixation bullseye changed to a filled circle target[22]. In Experiment 2, participants performed a categorization task with natural stimuli, classifying images based on the criterion "whether they are alive or not," as well as a passive viewing task, during which they viewed stimuli presented in rapid streams[23]. To investigate how electrode density influences decoding performance, we reanalyzed the 128-channel electroencephalography (EEG) data from both experiments using different electrode density configurations (16, 32, 64, 96, and 128 electrodes). We applied the exact analysis pipelines from the original studies to the reduced configurations, and summarise these analysis pipelines below.

2.1 Participants

Both experiments were conducted under local ethics committee approvals, and informed written consent was obtained from all participants. Experiment 1[22] involved 16 participants (11 females and 5 males, age range: 18 – 27 years), while Experiment 2[23] included 24 participants (15 females and 9 males, age range: 18 – 26 years).

2.2 Apparatus

In Experiment 1, stimuli were presented centrally with a visual angle of 6.5°, while in Experiment 2, the visual angle was approximately 5°. In both experiments, EEG data were recorded while participants viewed experimental stimuli presented on a monitor with a 60 Hz refresh rate. Recordings were acquired at a sampling rate of 1000 Hz using a 128-channel BrainVision ActiCap system (Brain Products GmbH). Electrode placement followed standard scalp configuration guidelines, using the international five percent system in both experiments[24]. EEG signals were referenced online to FCz.

2.3 Stimuli

Both original experiments utilized well-documented stimulus sets. As described in the

original study, the stimuli in Experiment 1[22] consisted of 256 oriented sinusoidal gratings generated using the GratingStim function in PsychoPy[25]. Each stimulus subtended 6.5° of visual angle and varied systematically along four visual feature dimensions: colour, spatial frequency, contrast, and orientation (Fig. 1A). Four levels were defined for each feature dimension. The four colours were RGB values ([66, 10, 104], [147, 38, 103], [221, 81, 58], [252, 165, 10]) that were approximately equidistant in colour space, and each was paired with its complementary colour. Orientations (22.5°, 67.5°, 112.5°, 157.5°) were evenly spaced circularly, while spatial frequencies (2.17, 1.58, 0.98, 0.39 cycles/°) and contrast values (0.9, 0.7, 0.5, 0.3) were linearly spaced. The resulting stimulus space included all 256 possible combinations. To prevent potential confounds related to phase, the phase of each grating was randomly varied on each presentation.

The stimuli in Experiment 2[23], as described in the original study, comprised 400 naturalistic colour images sourced from publicly available image databases (www.pixabay.com and www.pexels.com) under Creative Commons 0 licenses. All images were manually processed by the original authors using GIMP (v2.10.14)[26] to blur identifiable text (e.g., brand names) and were subsequently cropped and resized to approximately 5° of visual angle. The images were organized into six semantic categories based on Goldberg and Thompson-Schill[27]: animals (bee, cat, dog, dolphin, eagle, horse, lemur, pigeon, tiger, whale) and plants (cactus, clover, fern, flower, grass, lemon tree, moss, palm tree, tree, vine), which each included 10 objects. For all other categories, still artificial things (bench, clothes peg, headphones, lock, mug), still natural things (cliff, crystal, rock, sand, shell), moving artificial things (boat, bus, car, helicopter, train), and moving natural things (fire, hot spring, river, waterfall, waves), there were 5 objects. Within each category (e.g., cat, bench), there were 10 different images (e.g., cat1, cat2, … cat10). For objects capable of movement, the corresponding images depicted dynamic scenes (e.g., dolphins leaping out of the water, flowing waterfalls; see Fig. 1B), although all stimuli were presented as static images. Comprehensive information is provided in Shatek et al.[23].

2.4 EEG experiment procedure

Neural responses were collected using electroencephalography (EEG) while participants viewed experimental stimuli and performed specific tasks, following protocols from the original studies[22,23].

2.4.1 Experiment 1

Participants viewed sequences of 256 grating stimuli, each presented for 16.67 ms at either 6.67 Hz (150 ms SOA) or 20 Hz (50 ms SOA). Each sequence consisted of all 256 stimuli presented in random order, and 80 sequences were shown in total, with each stimulus repeated 40 times per frequency. A fixation bullseye appeared one second before each sequence and remained superimposed throughout. Participants pressed a button when the bullseye briefly changed to a filled circle, which occurred 2 – 4 times per sequence (Fig. 1C).

2.4.2 Experiment 2

Participants completed eight blocks alternating between an categorization task and a passive viewing task. For the current reanalysis, only the "alive" category task (2 blocks) and the passive viewing task (4 blocks) were included. To balance trial numbers across the six natural stimulus categories: living animals (whales), living plants (flowers), non-living moving artificial objects (trains), non-living moving natural objects (waterfalls), non-living still artificial objects (cups), and non-living still natural objects (rocks), half of the animal and plant trials were randomly selected.

For our reanalysis, in the "alive" task, 1200 trials (200 trials for each category) were divided into 10 sequences, each containing 120 trials, with 20 trials from each category. Each trial consisted of a fixation cross for a random duration between 500 ms and 1000 ms, followed by an image in the center of the screen for 100 ms. Participants had 1000 ms to judge whether the image depicted a living object. A response was confirmed by the fixation cross filling in; otherwise, the screen displayed "Too late!" (Fig. 1E). Similarly, in the passive viewing task, 3600 trials (600 trials per category) were divided into 10 sequences of 360 trials, each containing 60 trials per category. Each trial consisted of a 100 ms image presentation followed by a 50 ms inter-stimulus interval. Participants were instructed to monitor a fixation bullseye and respond by pressing a button whenever it changed color to red (Fig. 1D). For further procedural

details, see Shatek et al.[23].

2.5 EEG data analysis

2.5.1 EEG preprocessing

Preprocessed EEG data were obtained directly from the original datasets. As described in the source publication[22,23], signals had been re-referenced to the average reference, low-pass filtered at 100 Hz, high-pass filtered at 0.1 Hz, and down-sampled to 250 Hz. Epochs were constructed from 100 ms prior to 600 ms after each image presentation for Experiment 1, and from 300 ms before each stimulus appeared on the screen to 1000 ms after stimulus onset for Experiment 2. No further preprocessing steps were applied.

2.5.2 Stimulus decoding

To examine the effect of electrode density on decoding performance, we performed time-resolved multivariate pattern analysis (MVPA)[28] on preprocessed EEG data using CoSMoMVPA[29] in MATLAB. Neural responses were decoded at each time point for five electrode density levels (16, 32, 64, 96, and 128 electrodes), using subsets of electrodes sampled from the original 128-channel montage (Supplementary Table 1). Note that we followed standard configurations commonly used in low-density EEG devices, and ensured that electrode subsets were evenly distributed across the scalp (see Fig 2 head maps).

For Experiment 1, we decoded EEG epochs to grating stimuli varying across four visual features: orientation, contrast, spatial frequency, and color (each with four levels). For Experiment 2, we decoded six natural image categories: living animals (whales), living plants (flowers), non-living moving artificial objects (trains), non-living moving natural objects (waterfalls), non-living still artificial objects (cups), and non-living still natural objects (rocks). Regularized linear discriminant analysis (LDA) classifiers were trained and tested using a leave-one-sequence-out cross-validation procedure. For each fold, classifiers were trained on data from all but one sequence and tested on the held-out sequence, cycling through all sequences. Decoding accuracy was defined as the proportion of correctly classified trials and was assessed separately for each time point, visual feature or category, and electrode density. Performance was compared against theoretical chance levels (0.25 for grating features, 0.167 for natural image categories).

2.5.3 Statistical inference

To statistically assess whether group-level decoding accuracies exceeded chance, we computed Bayes factors[30-32], as implemented in the BayesFactor R package[33] and its corresponding implementation for time-series neuroimaging data[32]. The prior for the null hypothesis was set at chance level for decoding. The alternative hypothesis prior was an interval ranging from small effect sizes to infinity, accounting for small above-chance results as a result of noise[30,32].

The onset of above-chance decoding was defined as the first of three consecutive time points with BF > 10. To be able to compare onset and peak times, we calculated 95% confidence intervals by using a leave-two-participants-out jackknifing approach, where we calculated the onset and peak for all possible leave-two-out permutations (n = 120 for 16 participants in Experiment 1 and n = 276 for 24 participants in Experiment 2), and took the 95th percentile of the resulting distributions.

3. Results

To address how electrode density influences decoding performance, we systematically examined decoding accuracy across five electrode configurations (16, 32, 64, 96, and 128 channels) while decoding four levels of low-level visual grating features (orientation, contrast, spatial frequency, and color) in Experiment 1, and high-level natural image categories spanning six semantic classes in Experiment 2.

3.1 Dynamic visual grating feature coding

Using multivariate pattern analysis (MVPA), we successfully decoded feature-specific information for orientation, contrast, spatial frequency, and color at a presentation rate of 6.67 Hz across electrode densities ranging from 16 to 128 channels (Fig. 2, top panel). Notably, reliable decoding was achieved for all four features even with the lowest density of 16 electrodes. To evaluate temporal consistency across electrode densities, we examined group-level decoding onset (defined as three consecutive time points with Bayes factors >10) and peak decoding latency. For all four features, decoding onset consistently emerged before 90 ms post-stimulus across all configurations, while peak decoding latencies were clustered around 120 ms (Fig. 2, middle panel), indicating that the temporal dynamics of feature processing were largely preserved irrespective of channel count. Spatial consistency was further examined using topographical decoding maps. For all four features, decoding-related activity was consistently localized to occipital and parietal regions, with substantial spatial overlap observed across electrode densities (Fig. 2, head maps), suggesting a stable spatial topography of neural engagement. Finally, to quantify temporal profile similarity, we computed pairwise correlations of decoding time courses across all electrode configurations. Notably, the minimum correlation between the 16-electrode montage and higher-density configurations was significantly greater than 0.916 ($r = 0.916$ for orientation, 0.995 for spatial frequency, 0.992 for color, and 0.994 for contrast; all $p < 0.001$). This high degree of inter-density correlation (Fig. 2, bottom panel) reinforces the robustness and reproducibility of the decoding profiles. Together, these findings demonstrate that accurate, temporally consistent, and spatially overlapping decoding of multiple visual grating features is robust across electrode densities, including even the sparsest EEG

configurations, underscoring the efficiency of low-density EEG for neural decoding.

Next, we further examined whether these findings generalize to a faster stimulus presentation rate (20.00 Hz). Applying the same multivariate pattern analyses to stimuli presented at 20.00 Hz (Fig. 3), we observed similar decoding accuracy, timing, and spatial patterns across all electrode configurations. To assess temporal consistency across densities, we again computed pairwise correlations of the decoding time courses. Notably, the minimum correlation between the 16-electrode montage and higher-density configurations remained significantly high, with values of r = 0.814 for orientation, 0.996 for spatial frequency, 0.992 for color, and 0.987 for contrast (all $p < 0.001$). These findings confirm that decoding performance remains robust across electrode densities, even under accelerated stimulus presentation rates.

3.2 Dynamic natural stimuli coding

We next examined whether the decoding consistency across electrode densities extends to high-level, naturalistic visual input. To test this, we applied the same multivariate pattern analysis to EEG data collected during the viewing of natural images from six semantic categories: living animals (whales), living plants (flowers), non-living moving artificial objects (trains), non-living moving natural objects (waterfalls), non-living still artificial objects (cups), and non-living still natural objects (rocks). Analyses were conducted separately for the categorization task (Fig. 4A) and the passive viewing task (Fig. 4B), across five electrode densities (16, 32, 64, 96, and 128 channels).

In both tasks, decoding accuracy for object category was above chance across all electrode densities. Group-level decoding time courses revealed similar trajectories regardless of channel count, with decoding performance rising rapidly following stimulus onset and peaking between ~180–220 ms across all configurations (Fig. 4, top and middle panel). These results suggest that high-level semantic information, including animacy and object motion, is reliably encoded in EEG signals, even when recorded with a small number of electrodes. We further assessed spatial consistency using topographical decoding maps. For both tasks, decoding-related activity exhibited strong spatial overlap across electrode densities (Fig. 4, head maps), suggesting a stable spatial signature of categorical visual processing. To quantify the similarity of decoding

dynamics, we computed pairwise correlations of the time series across all five configurations. In both tasks, correlations were consistently high across electrode configurations (Fig. 4, bottom panel). The minimum correlation between the 16-electrode montage and higher-density configurations was 0.973 and 0.975 for the two tasks, respectively (all $p < 0.001$), confirming the robustness of temporal decoding profiles across varying densities. Together, these findings demonstrate that high-level visual information can also be accurately and consistently decoded from EEG signals even with sparse electrode configurations, further supporting the utility of low-density EEG for neural decoding.

4. Discussion

In this study, we systematically examined how varying EEG electrode densities influence neural decoding performance for both low-level (Experiment 1) and high-level (Experiment 2) visual stimuli. Remarkably, we found that decoding accuracy in temporal dynamics remained above chance even with as few as 16 electrodes, regardless of stimulus complexity or task demands. In addition, spatial patterns of decoding-related activity were broadly consistent across densities, suggesting a degree of spatial robustness. These findings highlight the reliability and generalizability of EEG-based neural decoding under sparse spatial sampling conditions.

Prior studies have suggested that increasing EEG electrode density enhances decoding accuracy, particularly for fine-grained perceptual task[10,11]. However, this does not imply that lower-density EEG cannot support decoding performance comparable to that of high-density systems. Recent findings[8,9,12] indicate that reliable decoding may still be possible with a reduced number of electrodes. Our results align with this emerging perspective by systematically offering evidence across a range of electrode configurations and stimulus types across both low- and high-level visual domains, unlike earlier studies that addressed only one level of stimulus complexity[8,10].

Although EEG signals originate from anatomically localized sources, such as early visual areas in the occipital cortex involved in encoding low-level features[13,34,35], they give rise to scalp potentials that are both locally enhanced and spatially distributed due to volume conduction[14-17]. Specifically, neural activity from focal sources propagates through the brain and skull, producing widespread scalp fields that extend well beyond the cortical origin. At the same time, these fields tend to exhibit maximal amplitude near their generating sources, which explains the consistently observed topography maps over occipital regions in Experiment 1. This dual property of EEG, global spread with regional specificity, enables sparse but widely distributed electrode arrays to capture the key components of multivariate signal patterns[8,9,12]. As long as the electrode montage ensures full-head coverage, even low-density configurations can retain sufficient information for effective decoding. Our findings support this principle: despite substantial reductions in electrode count, we observed reliable decoding of both

temporal dynamics and spatial structures, across both low- and high-level visual tasks.

A key strength of this study lies in the systematic manipulation of electrode density across two distinct experimental datasets, which provides robust validation of the findings. One limitation, however, is that the electrode positions in the reduced-density setups were fixed and based on standard EEG configurations, rather than being optimized for individual participants or task demands. To fully leverage the benefits of using a smaller number of electrodes, future studies could explore individualized electrode selection strategies, for example, selecting the most informative channels based on subject-specific signal-to-noise ratios, decoding performance, or task-related activation patterns[36].

Our results demonstrated that reliable decoding can be achieved with fewer electrodes, which supported the broadly distributed activities across the whole brain and opened new possibilities for scalable applications such as mobile brain-computer interfaces, clinical monitoring, and real-world cognitive assessment[37-40]. These findings carry important implications for the development of portable and cost-effective EEG systems.

Figure legends

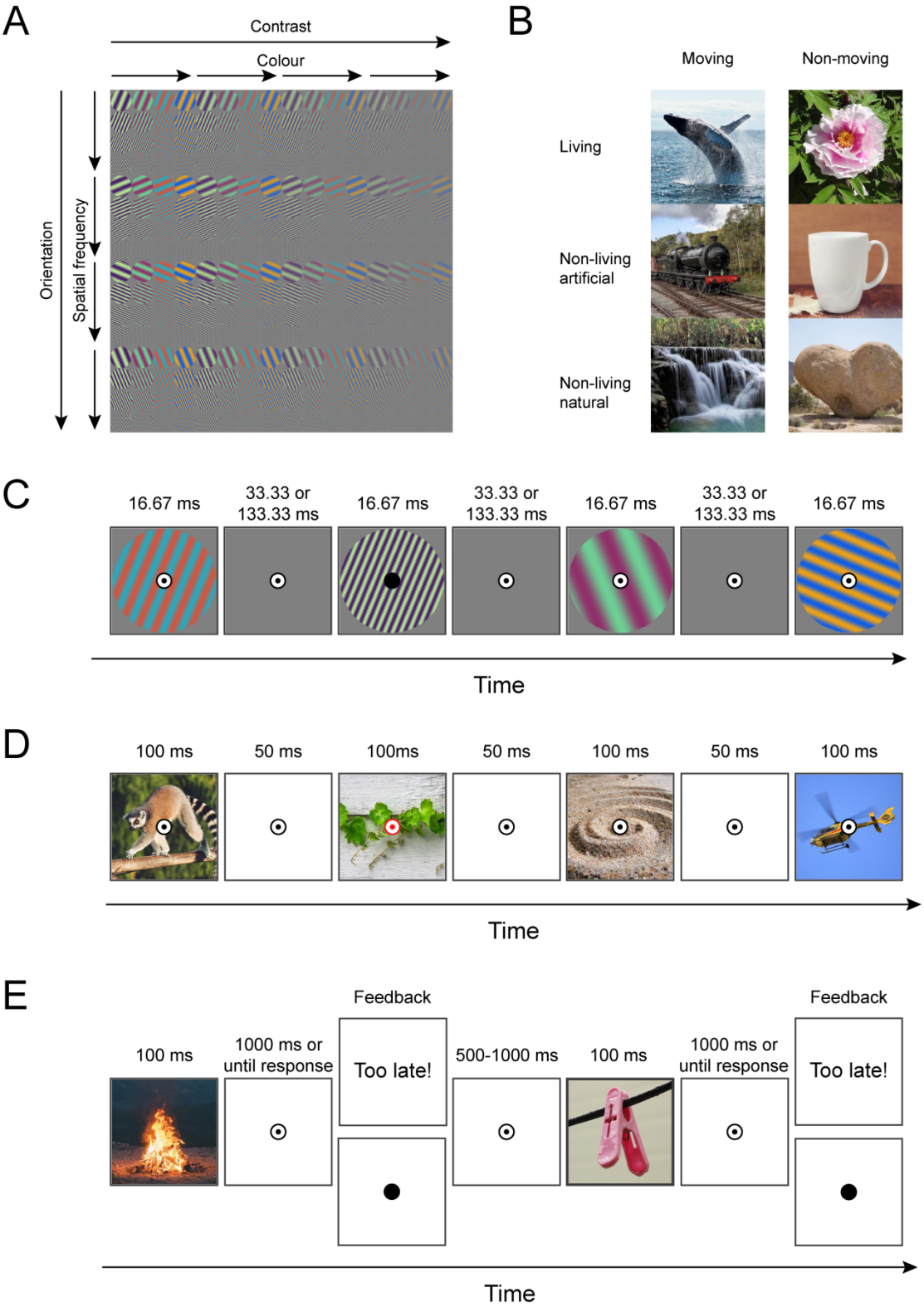

Figure 1. Experimental paradigm for Experiments 1 and 2 with EEG. Sample stimuli are shown in (A) for Experiment 1 and (B) for Experiment 2. In Experiment 1, visual grating stimuli were presented for one frame (16.67 ms) at 6.67 Hz (133 ms ISI; 150

ms SOA) or 20 Hz (33 ms ISI; 50 ms SOA). Participants were asked to detect when the fixation bullseye changed to a filled circle target and respond using a button press. In Experiment 2, during passive viewing trials (D), participants viewed a rapid stream of natural images and responded by pressing a button when the fixation spot changed to red. During categorisation trials (E), participants categorised images based on whether each depicted something alive or not alive. Note that all images are magnified here for clarity; in the actual presentation, they occupied a smaller proportion of the screen. Panels (A) and (C) are adapted from Grootswagers et al.[22], while Panels (B), (D), and (E) are adapted from Shatek et al. [23].

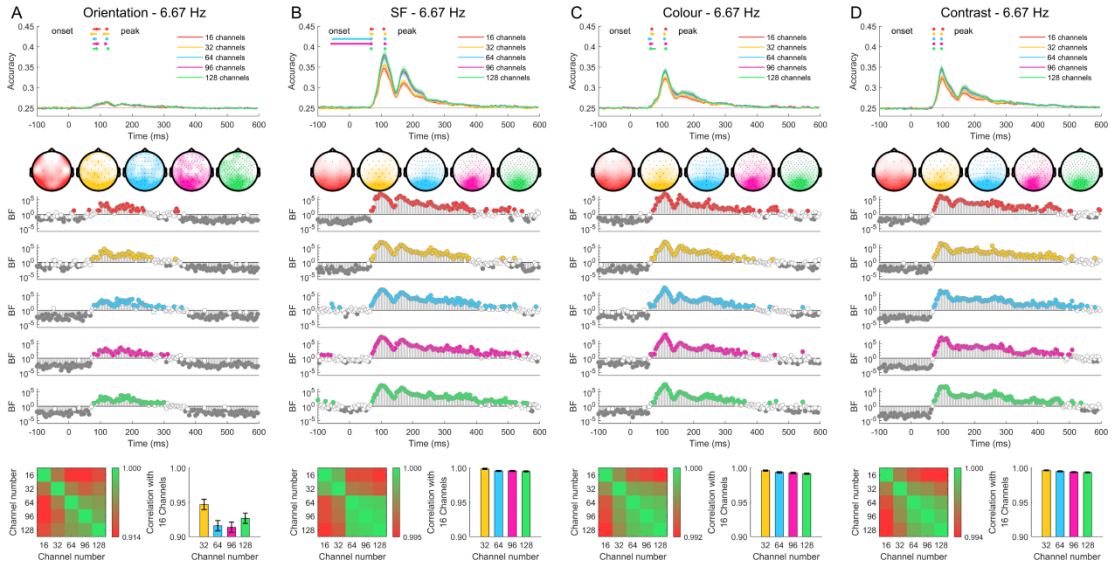

Figure 2. Dynamics of visual coding for orientation, spatial frequency, colour, and contrast at a 6.67 Hz stimulus presentation rate with varying electrode density. (A) The time course of decoding accuracy for orientation with varying electrode density at a 6.67 Hz presentation rate. Confidence intervals for the onsets and peaks of individual electrode densities are plotted above the decoding traces. The head maps illustrate the channel clusters with the highest feature information at the peak of decoding, based on results from a channel searchlight analysis. Bayes Factors for classification evidence compared to chance (0.25) are plotted below. In the bottom row, the correlation coefficient matrix across different electrode densities and the corresponding correlation coefficient bar plot are displayed. (B–D) Same as (A), but for spatial frequency (B), colour (C), and contrast (D).

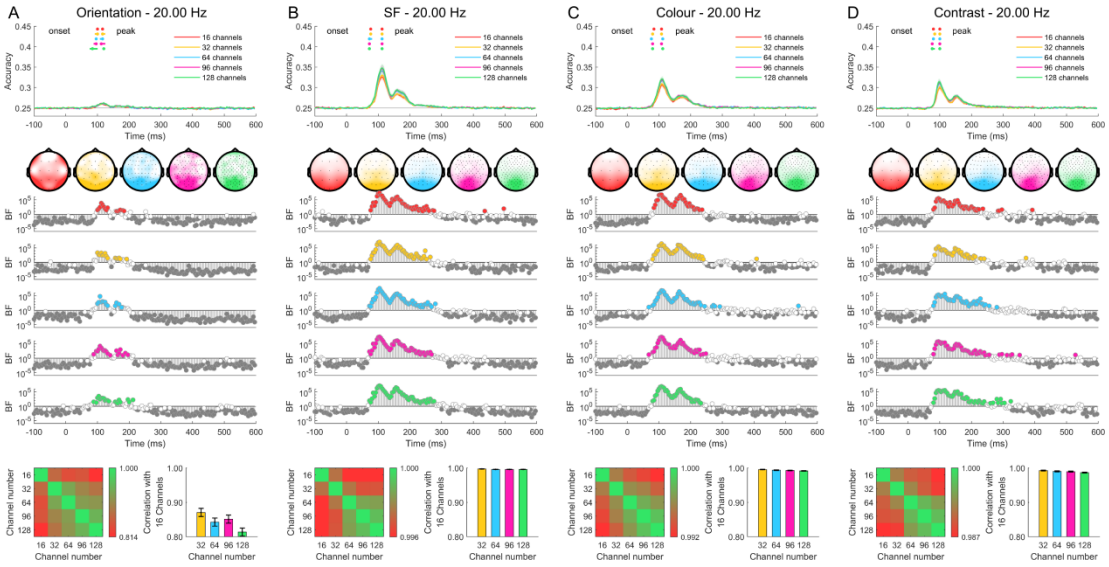

Figure 3. Dynamics of visual coding for orientation, spatial frequency, colour, and contrast at a 20.00 Hz stimulus presentation rate with varying electrode density. (A) The time course of decoding accuracy for orientation with varying electrode density at a 20.00 Hz presentation rate. Confidence intervals for the onsets and peaks of individual electrode densities are plotted above the decoding traces. The head maps illustrate the channel clusters with the highest feature information at the peak of decoding, based on results from a channel searchlight analysis. Bayes Factors for classification evidence compared to chance (0.25) are plotted below. In the bottom row, the correlation coefficient matrix across different electrode densities and the corresponding correlation coefficient bar plot are displayed. (B–D) Same as (A), but for spatial frequency (B), colour (C), and contrast (D).

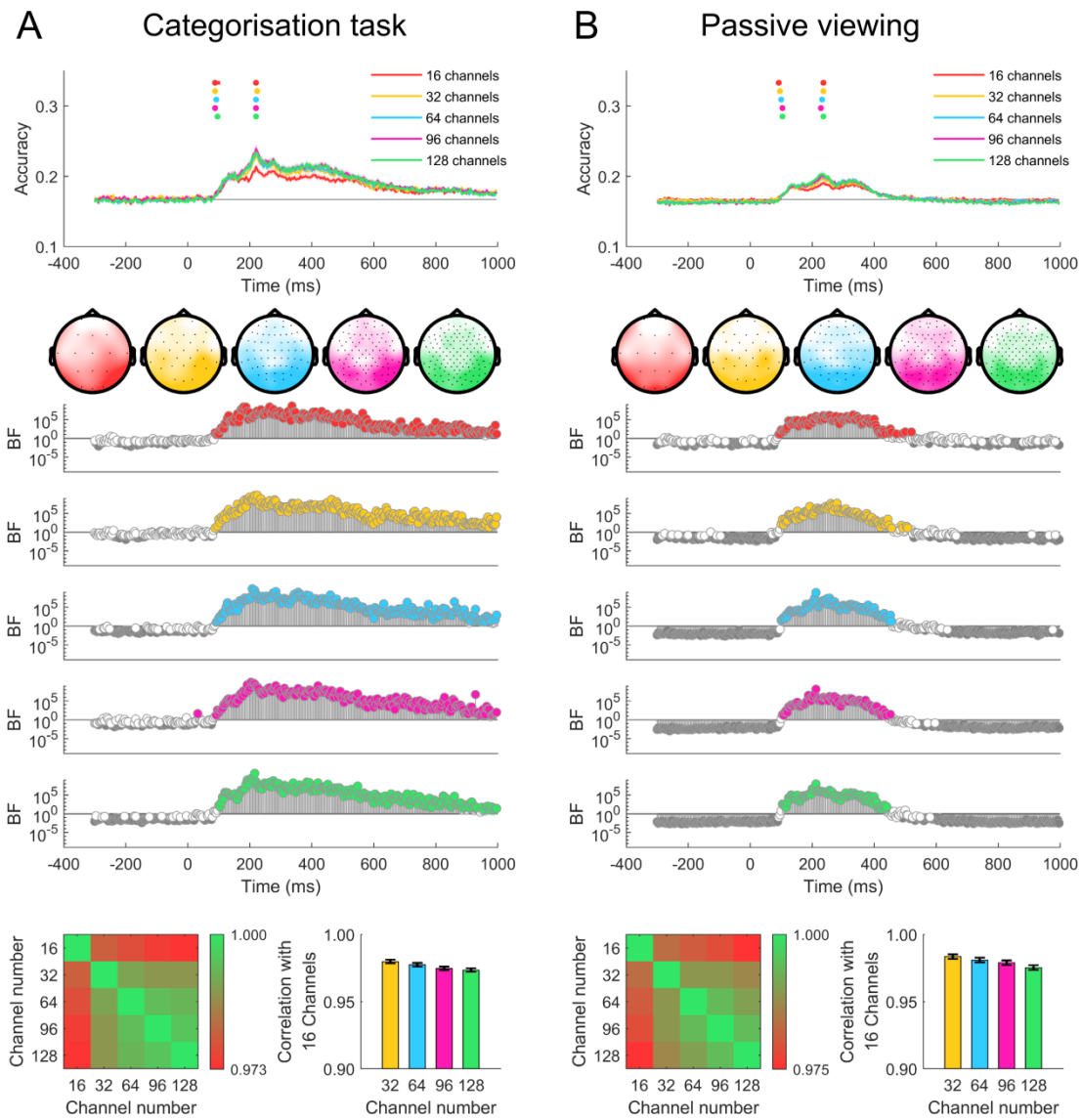

Figure 4. Dynamics of visual coding for natural stimuli at categorisation and passive viewing tasks with varying electrode density. (A) The time course of decoding accuracy at categorisation task with varying electrode density. Confidence intervals for the onsets and peaks of individual electrode densities are plotted above the decoding traces. The head maps illustrate the channel clusters with the highest categorical information at the peak of decoding, based on results from a channel searchlight analysis. Bayes Factors for classification evidence compared to chance (0.167) are plotted below. In the bottom row, the correlation coefficient matrix across different electrode densities and the corresponding correlation coefficient bar plot are displayed. (B) Same as (A), but at passive viewing task.

Data and Code Availability

This study utilized publicly available datasets from OpenNeuro: Experiment 1 (https://doi.org/10.18112/openneuro.ds004357.v1.0.1) and Experiment 2 (https://doi.org/10.18112/openneuro.ds003885.v1.0.7). Code is publicly available at https://osf.io/xu2he/

Author contributions

Conceptualization, L.H., M.V., T.G.; Methodology, L.H., T. G.; Formal Analysis, L.H.; Visualization L.H.; Writing – Original Draft, L. H.; Writing – Review and Editing, L. H., M.V., T. G.

Funding

This work was supported by ARC DE230100380 (T. G.), ARC DP220103047 (M. V.), and a MARCS international visiting scholarship (L. H.).

Ethics Statement

This work uses only publicly available datasets. No ethics approval was required.

Declaration of Competing Interests

The authors declare no competing interests.

References

1. Niedermeyer, E., & da Silva, F. L. (Eds.). *Electroencephalography: basic principles, clinical applications, and related fields*. Lippincott Williams & Wilkins. (2005).
2. Bae, G. Y., & Luck, S. J. Dissociable decoding of spatial attention and working memory from EEG oscillations and sustained potentials. *Journal of Neuroscience*, **38**, 409–422. (2018).
3. Bae, G. Y., & Luck, S. J. Decoding motion direction using the topography of sustained ERPs and alpha oscillations. *NeuroImage*, **184**, 242–255. (2019).
4. Grootswagers, T., Robinson, A. K., & Carlson, T. A. The representational dynamics of visual objects in rapid serial visual processing streams. *NeuroImage*, **188**, 668–679. (2019).
5. Isik, L., Meyers, E. M., Leibo, J. Z., & Poggio, T. The dynamics of invariant object recognition in the human visual system. *Journal of neurophysiology*, **111**, 91–102. (2014).
6. Robinson, A. K., Grootswagers, T., & Carlson, T. A. The influence of image masking on object representations during rapid serial visual presentation. *NeuroImage*, **197**, 224–231. (2019).
7. Song, Y., Liu, B., Li, X., Shi, N., Wang, Y., & Gao, X. Decoding natural images from eeg for object recognition. *arXiv preprint arXiv:2308.13234*. (2023).
8. Guenther, S., Kosmyna, N., & Maes, P. Image classification and reconstruction from low-density EEG. *Scientific Reports*, **14**, 16436. (2024).
9. Meng, J., Edelman, B. J., Olsoe, J., Jacobs, G., Zhang, S., Beyko, A., & He, B. A study of the effects of electrode number and decoding algorithm on online EEG-based BCI behavioral performance. *Frontiers in neuroscience*, **12**, 227. (2018).
10. Robinson, A. K., Venkatesh, P., Boring, M. J., Tarr, M. J., Grover, P., & Behrmann, M. Very high density EEG elucidates spatiotemporal aspects of early visual processing. *Scientific reports*, **7**, 16248. (2017).
11. Michel, C. M., & Murray, M. M. Towards the utilization of EEG as a brain imaging tool. *Neuroimage*, **61**, 371–385. (2012).
12. Nguyen-Danse, D. A., Singaravelu, S., Chauvigné, L. A., Mottaz, A., Allaman, L.,

& Guggisberg, A. G. Feasibility of reconstructing source functional connectivity with low-density EEG. *Brain Topography*, **34**, 709–719. (2021).

13. Hubel, D. H., & Wiesel, T. N. Receptive fields and functional architecture in two nonstriate visual areas (18 and 19) of the cat. *Journal of neurophysiology*. (1965).
14. Nunez, P. L., & Srinivasan, R. *Electric fields of the brain: the neurophysics of EEG*. Oxford university press. (2006).
15. Pizzagalli, D. A. Electroencephalography and high-density electrophysiological source localization. *Handbook of psychophysiology*, **3**, 56–84. (2007).
16. Van den Broek, S. P., Reinders, F., Donderwinkel, M., & Peters, M. J. Volume conduction effects in EEG and MEG. *Electroencephalography and clinical neurophysiology*, **106**, 522–534. (1998).
17. Vorwerk, J., Cho, J. H., Rampp, S., Hamer, H., Knösche, T. R., & Wolters, C. H. A guideline for head volume conductor modeling in EEG and MEG. *NeuroImage,* **100**, 590–607. (2014).
18. Michel, C. M., Murray, M. M., Lantz, G., Gonzalez, S., Spinelli, L., & De Peralta, R. G. EEG source imaging. *Clinical neurophysiology*, **115**, 2195–2222. (2004).
19. Leeb, R., Perdikis, S., Tonin, L., Biasiucci, A., Tavella, M., Creatura, M., ... & dR Millán, J. Transferring brain–computer interfaces beyond the laboratory: successful application control for motor-disabled users. *Artificial intelligence in medicine*, **59**, 121–132. (2013).
20. Koutroumanidis, M., Arzimanoglou, A., Caraballo, R., Goyal, S., Kaminska, A., Laoprasert, P., ... & Moshé, S. L. The role of EEG in the diagnosis and classification of the epilepsy syndromes: a tool for clinical practice by the ILAE Neurophysiology Task Force (Part 1). *Epileptic Disorders*, **19**, 233–298. (2017).
21. Wilmshurst, J. M., Gaillard, W. D., Vinayan, K. P., Tsuchida, T. N., Plouin, P., Van Bogaert, P., ... & Cross, J. H. Summary of recommendations for the management of infantile seizures: Task force report for the ILAE commission of pediatrics. *Epilepsi*a, **56**, 1185–1197. (2015).
22. Grootswagers, T., Robinson, A. K., Shatek, S. M., & Carlson, T. A. Mapping the dynamics of visual feature coding: Insights into perception and integration. *PLOS*

Computational Biology, **20**, e1011760. (2024).

23. Shatek, S. M., Robinson, A. K., Grootswagers, T., & Carlson, T. A. Capacity for movement is an organisational principle in object representations. *NeuroImage*, **261**, 119517. (2022).
24. Oostenveld, R., & Praamstra, P. The five percent electrode system for high-resolution EEG and ERP measurements. *Clinical neurophysiology*, **112**, 713–719. (2001).
25. Peirce, J., Gray, J. R., Simpson, S., MacAskill, M., Höchenberger, R., Sogo, H., ... & Lindeløv, J. K. PsychoPy2: Experiments in behavior made easy. *Behavior research methods*, **51**, 195–203. (2019).
26. Grootswagers, T. A primer on running human behavioural experiments online. *Behavior research methods*, **52**, 2283–2286. (2020).
27. Goldberg, R. F., & Thompson-Schill, S. L. Developmental "roots" in mature biological knowledge. *Psychological Science*, **20**, 480–487. (2009).
28. Grootswagers, T., Wardle, S. G., & Carlson, T. A. Decoding dynamic brain patterns from evoked responses: A tutorial on multivariate pattern analysis applied to time series neuroimaging data. *Journal of cognitive neuroscience*, **29**, 677–697. (2017).
29. Oosterhof, N. N., Connolly, A. C., & Haxby, J. V. CoSMoMVPA: multi-modal multivariate pattern analysis of neuroimaging data in Matlab/GNU Octave. *Frontiers in neuroinformatics*, **10**, 27. (2016).
30. Morey, R. D., & Rouder, J. N. Bayes factor approaches for testing interval null hypotheses. *Psychological methods*, **16**, 406. (2011).
31. Rouder, J. N., Speckman, P. L., Sun, D., Morey, R. D., & Iverson, G. Bayesian t tests for accepting and rejecting the null hypothesis. *Psychonomic bulletin & review*, **16**, 225–237. (2009).
32. Teichmann, L., Moerel, D., Baker, C., & Grootswagers, T. An Empirically Driven Guide on Using Bayes Factors for M/EEG Decoding. *Aperture Neuro*, **2**, 1–10. (2022).
33. Morey, R. D., & Rouder, J. N. BayseFactor: computation of bayes factors for common designs. (2018).

34. Huang, L., Wang, L., Shen, W., Li, M., Wang, S., Wang, X., ... & Zhang, X. A source for awareness-dependent figure–ground segregation in human prefrontal cortex. *Proceedings of the National Academy of Sciences*, **117**, 30836–30847. (2020).
35. Wang, J., Shi, L., Wang, W., & Hou, Z. G. Efficient brain decoding based on adaptive EEG channel selection and transformation. *IEEE Transactions on Emerging Topics in Computational Intelligence*, **6**, 1314-1323. (2022).
36. Wang, L., Huang, L., Li, M., Wang, X., Wang, S., Lin, Y., & Zhang, X. An awareness-dependent mapping of saliency in the human visual system. *NeuroImage*, **247**, 118864. (2022).
37. Grootswagers, T., Quek, G. L., Zeng, Z., & Varlet, M. Human infant EEG recordings for 200 object images presented in rapid visual streams. *Scientific Data*, **12**, 407. (2025).
38. Moerel, D., Grootwagers, T., Quek, G. L., Smit, S., & Varlet, M. Unlocking information alignment between interacting brains with EEG hyperscanning. *bioRxiv*, 2025-01. (2025).
39. Rudroff, T. Decoding thoughts, encoding ethics: A narrative review of the BCI-AI revolution. *Brain Research*, **1850**. (2024).
40. Varlet, M., & Grootswagers, T. Measuring information alignment in hyperscanning research with representational analyses: Moving beyond interbrain synchrony. *Frontiers in Human Neuroscience,* **18**, 1385624. (2024).